catalysts

MDPI

Article

Assessment of a Novel Photocatalytic TiO_2-Zirconia Ultrafiltration Membrane and Combination with Solar Photo-Fenton Tertiary Treatment of Urban Wastewater

Dennis Deemter [1], Fabricio Eduardo Bortot Coelho [2], Isabel Oller [1], Sixto Malato [1,*] and Ana M. Amat [3]

[1] Plataforma Solar de Almería-CIEMAT, Carretera de Senés Km 4, Tabernas, 04200 Almería, Spain; ddeemter@psa.es (D.D.); isabel.oller@psa.es (I.O.)
[2] Department of Chemistry, University of Turin, Via P. Giuria 7, 10125 Torino, Italy; fabricioeduardo.bortotcoelho@unito.it
[3] Grupo Procesos de Oxidación Avanzada, Campus de Alcoy, Universitat Politècnica de València, 03801 Alcoy, Spain; aamat@txp.upv.es
* Correspondence: sixto.malato@psa.es

Abstract: The objective of this study was to assess the combination of a photocatalytic TiO_2-coated ZrO_2 UF membrane with solar photo-Fenton treatment at circumneutral pH for the filtration and treatment of urban wastewater treatment plant (UWWTP) effluents. Photocatalytic self-cleaning properties were tested with a UWWTP effluent under irradiation in a solar simulator. Then, both the permeates and retentates from the membrane process were treated using the solar photo-Fenton treatment. The UWWTP effluent was spiked with caffeine (CAF), imidacloprid (IMI), thiacloprid (THI), carbamazepine (CBZ) and diclofenac (DCF) at an initial concentration of 100 µg/L each. Retention on the membrane of *Pseudomonas Aeruginosa (P. Aeruginosa)*, a Gram-negative bacterial strain, was tested with and without irradiation. It was demonstrated that filtration of a certain volume of UWWTP effluent in the dark is possible, and the original conditions can then be recovered after illumination. The photocatalytic membrane significantly reduces the turbidity of the UWWTP effluent, significantly increasing the degradation efficiency of the subsequent solar photo-Fenton treatment. The results showed that the membrane allowed consistent retention of *P. Aeruginosa* at an order of magnitude of 1×10^3–1×10^4 CFU/mL.

Keywords: advanced oxidation processes; bacteria retention; photocatalytic membranes; photo-induced super-hydrophilicity; titania; ZrO_2

Citation: Deemter, D.; Coelho, F.E.B.; Oller, I.; Malato, S.; Amat, A.M. Assessment of a Novel Photocatalytic TiO_2-Zirconia Ultrafiltration Membrane and Combination with Solar Photo-Fenton Tertiary Treatment of Urban Wastewater. *Catalysts* **2022**, *12*, 552. https://doi.org/10.3390/catal12050552

Academic Editor: Antonio Eduardo Palomares

Received: 19 April 2022
Accepted: 16 May 2022
Published: 18 May 2022

1. Introduction

Membranes have proven to be economic, fast and reliable solutions for the world's increasing water contamination problems. These vast and growing problems are due to the increasing use of pesticides and other chemicals known as microcontaminants (MCs), which are usually found in the already limited fresh water supply and agricultural lands, combined with salination [1–3]. MCs are found at trace levels up to significant concentrations, accumulating in wastewater streams and bodies, especially urban wastewater treatment plant (UWWTP) effluent and groundwater. As they are usually within the range of ng/L to µg/L, they often pass through conventional water treatment methods without being treated or recorded. These Contaminants of Emerging Concern (CECs) are found worldwide but are not yet regulated [4,5].

CECs can be removed from UWW with advanced oxidation processes (AOPs), which by generating highly reactive and nonselective hydroxyl radicals (•OH), can be applied for the elimination of MCs in a wide variety of UWWs, such as ozonation, photo-Fenton or electrooxidation processes [6–8]. On the other hand, other technologies have also been used successfully to remove pharmaceuticals contained in the UWWTP effluents, especially

the membrane system and AOP combination. Membrane systems are known to be very efficient in the retention of microcontaminants due to their physicochemical properties, although a concentrate stream is also generated. Therefore, the management and treatment of the concentrate are likely to be key components for reducing the environmental impacts of wastewater reclamation [9].

The two main categories of membrane materials are polymers and ceramics [10]. They both have distinctive characteristics that control and enable the optimization of overall system parameters, such as the flow rate, pressure and temperature, depending on the treatment being applied to general volumes or specific batches. Polymeric membranes are currently the most widely used in water treatment, but they have major mechanical, thermal, pH and chemical resistance drawbacks. Ceramic membranes, although more expensive, have superior resistance [11–13]. Both types of membrane are subject to fouling and the formation of either inorganic or organic material on the membrane surface. Biofouling involves the deposition of bacteria and other microorganisms that often produce a matrix of extra-cellular polymeric substances on the membrane surface [1,14–16].

Another solution for reducing membrane fouling, as well as for the further treatment of the resulting volumes after filtration, involves the abovementioned AOPs. Photocatalysis via the illumination of semiconductors with light at wavelengths with enough energy to trigger charge (e^- and h^+) separation is a well-known AOP. Photocatalytically active nanoparticles of TiO_2 (titania), ZrO_2, ZnO or WO_3 immobilized on a (membrane) surface can act as photocatalysts in the formation of these $^{\bullet}OH$, and have the advantage of not having to be filtered out or separated after the treatment [17]. As the overall efficiency of the supported semiconductors is low, although it might be enough to avoid biofouling, it is not enough for the elimination of MCs present in membrane influent. Therefore, other AOPs have to be applied to treat membrane effluents, as noted before.

In photo-Fenton treatment, a catalytic iron cycle (Fe^{2+}/Fe^{3+}) is stimulated by H_2O_2 and UV–Vis light to produce $^{\bullet}OH$. This treatment is of special interest as it can be driven by solar irradiation [18–20]. One of the main drawbacks of classic solar photo-Fenton treatment is that its optimal pH is below 3. At higher pH levels, the iron precipitates as ferric hydroxide. A complexing agent, such as ethylenediamine-*N*, *N*′-disuccinic acid (EDDS), a nontoxic biodegradable complexing agent that is able to keep the iron dissolved at up to pH9, can be used to avoid this [21–23].

Bacteria such as *E. Coli* and *P. Aeruginosa* found in UWWTP effluents can cause severe illness when ingested. Furthermore, effluents containing high concentrations of these bacteria and MCs, when simply discharged in nature or reused for crop irrigation, can become further multidrug-resistant when exposed to other untreated MCs [24–26]. Therefore, effective bacteria removal must be part of any application for its reuse [27]. The proper combination of membrane systems and AOPs could solve biofouling, MC removal and disinfection issues, permitting the consistent reuse of UWWTP effluents.

The objective of this study was to assess the combination of a photocatalytic TiO_2-coated ZrO_2 UF membrane developed in a previous study [28] with solar photo-Fenton treatment at circumneutral pH for the filtration of UWWTP effluents. Therefore, batches of UWWTP effluents were ultra-filtered using photocatalytic membranes and then treated via solar photo-Fenton treatment. First, the photocatalytic self-cleaning properties were tested with a UWWTP effluent under irradiation in a solar simulator. Then, both the permeates and retentates from membrane process were treated via solar photo-Fenton treatment, using EDDS as an iron complexing agent and hydrogen peroxide or persulfate as oxidants. The aim throughout was a total MC elimination rate of 80%, as per Swiss treatment regulations for UWWTP effluents, which are the first such regulations worldwide [29]. Matrices were spiked with a variety of MCs, caffeine (CAF), imidacloprid (IMI), thiacloprid (THI), carbamazepine (CBZ) and diclofenac (DCF), all frequently found in UWWTP effluents, at an initial concentration of 100 µg/L each. Retention on the membrane of *Pseudomonas Aeruginosa* (*P. Aeruginosa*), a Gram-negative, rod-shaped bacterium, was tested with and without irradiation to assess possible future applications for this novel photocatalytic

UF membrane as a (pre)filtration treatment of UWWTP effluents. *P. Aeruginosa* is an opportunistic multidrug-resistant bacterium that is commonly used as a model due to its ability to colonize medical equipment and its association with human diseases. It is able to interact with other bacteria, fungi and viruses; possesses mutational resistance mechanisms; and is known for its biofilm growth, even on inert materials [26,30–32].

2. Materials and Methods

2.1. Reagents and Chemicals

The UWWTP effluent was taken after secondary treatment in the 'El Bobar' UWWTP located in southeast Spain (Almeria) (see Table S1 for physicochemical characterization). Sigma Aldrich supplied $Fe_2(SO_4)_3 \cdot xH_2O$ for Fe(III)) and the HPLC-grade solvents for MC monitoring. MCs were obtained mainly from Sigma Aldrich (IMI, THI, CBZ and DCF), whereas CAF was supplied by Fluka. The reagents, H_2O_2 (35% *w*/*v*) and sodium persulfate ($Na_2S_2O_8$), were also purchased from Sigma Aldrich. A schematic overview of the five selected MCs is shown in Table S2. UPLC column retention time, LOQ and maximum contaminant absorption data are summarized in Table S3. Type CM0067 Nutrient Broth No. 2 was supplied by OXCID LTD., England, and the Pseudomonas Chromogenic Agar by Condalab, Spain, whereas the *Pseudomonas Aeruginosa* was from the Spanish Culture Collection (CECT).

2.2. Analytical Determinations

Scanning electron microscopy (SEM) images were taken with a Zeiss Sigma 300 VP Gemini Technology electron microscope at variable pressure. The SEM was equipped for energy-dispersive X-ray spectroscopy (EDX) to determine the chemical composition of the ceramic membrane samples by identifying the elements present, along with their concentration and distribution. Concentrations of selected MCs were determined by ultra-performance liquid chromatography (UPLC) using an Agilent Technologies 1200 series device equipped with a UV-DAD detector and Poroshell 120 EC-C18 column (3.0 × 50 mm). Eluent conditions started from 95% water with 25 mM formic acid (mobile phase A) and 5% acetonitrile (ACN) (mobile phase B) at 1 mL/min for 5 min. This was followed by a 10 min linear gradient to 68% ACN, which was maintained for 2 min. The working temperature was 30 °C and the injection volume was 100 µL. The samples prepared at a 1:9 ACN ratio were mixed and filtered through a hydrophobic PTFE 0.2 µm (Millipore Millex-FG) syringe filter into a 2 mL HPLC vial. Molecular weight, UPLC column retention time, LOQ and maximum contaminant absorption data are given in Table S3. Dissolved organic carbon (DOC) and inorganic carbon values were determined using a Shimadzu TOC-VCN analyzer. H_2O_2 values were determined according to DIN 38402H15 with titanium (IV) oxysulfate. Iron values were determined after filtration through a 0.45 µm nylon filter using 1,10 phenanthroline according to ISO 6332. The Liang method [33] was adapted to persulfate determination. Turbidity was measured using a Hach 2100N Turbidimeter. Total suspended solids (TSS) were measured via filtration without binder through a predried and weighed GF 52 090 Glass Microfiber Filter from ALBET LabScience, Germany. The filter paper was then placed in an oven at 105 °C for 60 min. Bacteria were cultured in a Series BD standard incubator at 36 °C.

2.3. Experimental Setup

The UWWTP effluent was filtered through a photocatalytic ceramic ZrO_2 ultrafiltration flat-sheet membrane designed and fabricated in a previous study. The membrane consists of a 100 ± 1-mm-wide, 150 ± 2-mm-long, highly porous, multi-channeled SiC support with 25 2 × 2 mm channels and 15 µm pore size supplied by LiqTech Ceramics A/S (Ballerup, Denmark). This is followed by a ZrO_2/SiC intermediate layer with 60 nm pores, covered with a wash coating of TiO_2 particles with a mean size of 10 nm. Membrane function follows the submerged outside-in filtration principle and is able to operate in a pH range of 0–14. Further details are described elsewhere [28]. SEM images of a cut surface can be

seen in Figure 1. Only the irradiated side of the membrane was left open; the remaining sides and bottom of the membrane were covered with a watertight polymer film to ensure that the permeation flow rate was only measured on the 150 cm^2 irradiated surface. The membrane was held in place by a fixture to provide an evenly divided crossflow over both membrane surfaces and was placed on the bottom of a 6 L container. The container was then positioned in a SunTest XLS+ solar simulator, containing a xenon lamp with daylight filter, providing a total light irradiation of 365 W/m^2 (300–800 nm), with a total UV radiation of 30 W/m^2 (300–400 nm), while the temperature was kept at 25 °C. A vacuum was created in the membrane support with a Watson Marlow 520 S peristaltic pump through a MARPRENE 902.0048.016 #25 tube at 20 rpm to obtain the permeate volume (see Figure 2 for a schematic view). The MC mixture containing CAF, IMI, THI, CBZ and DCF in methanol had previously been prepared as a stock solution. Each compound had a final concentration of 2.5 g/L to ensure solubility and low DOC. The UWWTP effluent was spiked with this stock solution to a final concentration of 100 µg/L per MC.

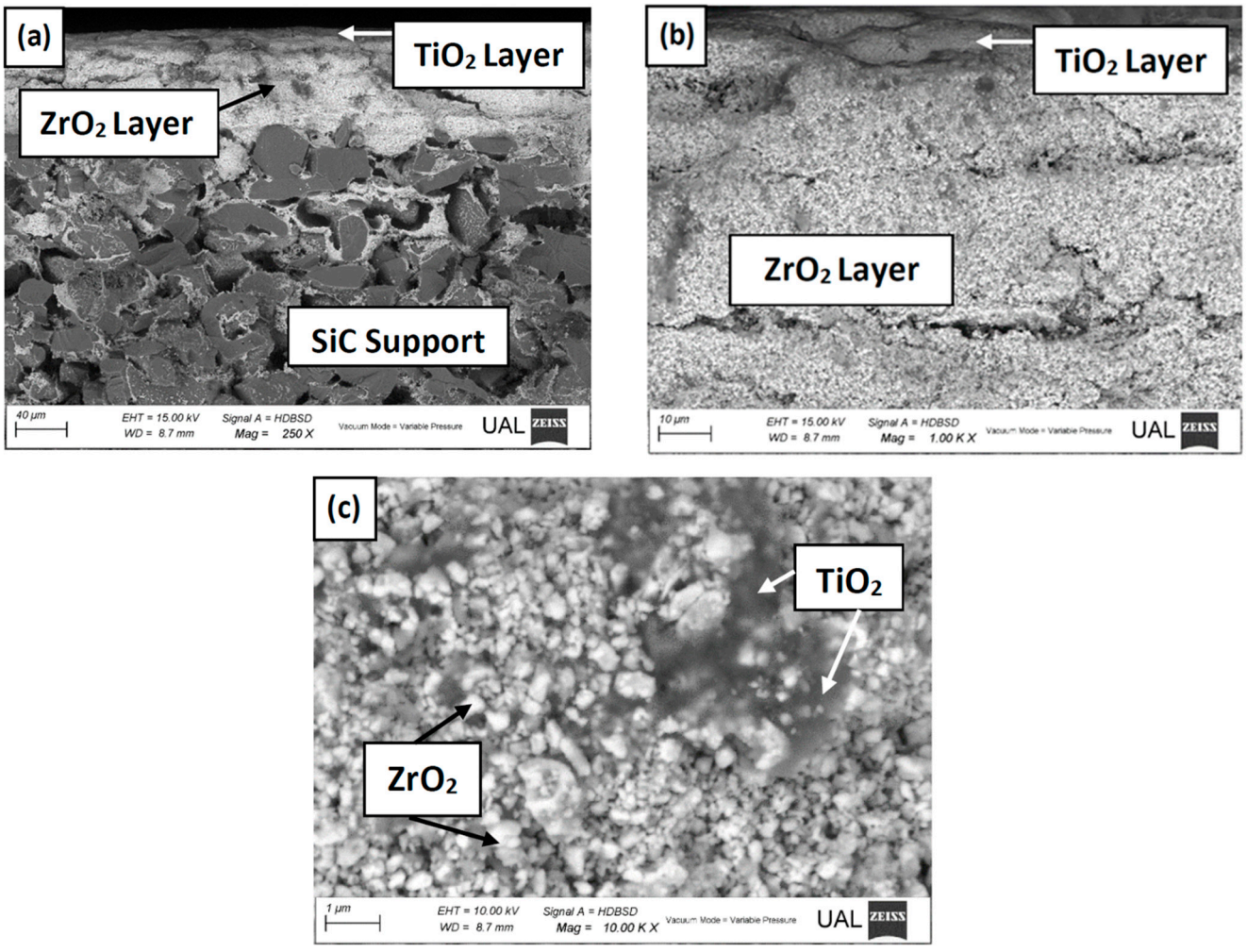

Figure 1. SEM images of a cross-section of the membrane: (**a**) the triple-layer membrane construction, showing the SiC support in grey, followed by the ZrO_2 intermediate UF membrane layer, while the grey shadows on top are the TiO_2 wash coating; (**b**) side view and (**c**) top view, showing the intermediate ZrO_2 UF membrane layer covered by the TiO_2 wash coating. The presence of the ZrO_2 and the TiO_2 wash coating was confirmed by EDX.

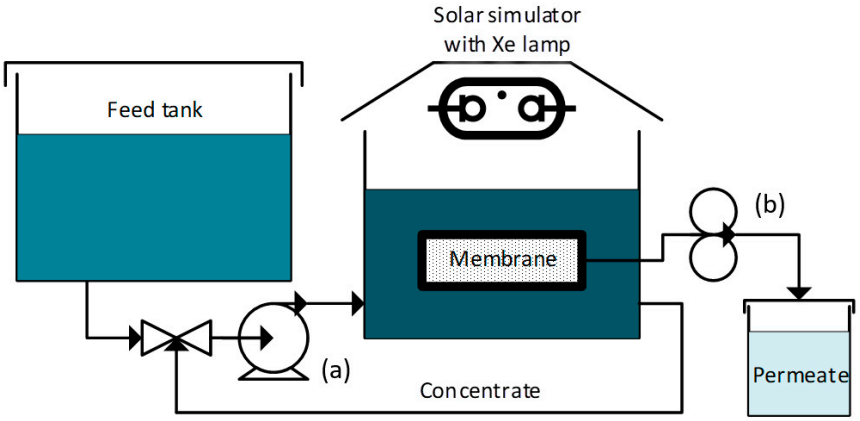

Figure 2. Schematic overview of the experimental set-up, with a recirculating pump (**a**) and a peristaltic pump (**b**), creating a vacuum in the membrane support to generate flow.

2.3.1. Solar Photo-Fenton Treatment

Solar photo-Fenton experiments were performed in the solar simulator described above, using a cylindrical 1 L container as the reactor (18.5 cm diameter and 4.0 cm depth), which was held in place and stirred magnetically in the center of the solar simulator. In selected experiments, the bicarbonates, known to be •OH radical scavenger, naturally present in UWWTP effluents, were air-stripped from the experimental volumes before starting the solar photo-Fenton treatments by adding H_2SO_4 to lower the concentration of HCO_3^- to 75 mg/L. The Fe^{3+}:EDDS complex was formed by predissolving $Fe_2(SO_4)_3.7H_2O$ in demineralized water at pH 3, followed by the addition of EDDS. A ratio of 1:1 was maintained during all experiments and the starting reagent concentration was 1.50 mM for both H_2O_2 and persulfate. Table S4 summarizes the experiments.

2.3.2. Retention of *P. Aeruginosa*

The membrane was placed in the container as described above, and the system was sterilized with H_2O_2 to ensure that there were no living bacteria in it. In this case, the water matrix was 5 L of natural water (Tabernas, southeast Spain). The *P. Aeruginosa* inoculum was prepared 20 h prior to the start of experiment and added to the reactor at a concentration of 1×10^6 CFU/mL, which is known for its predominant bacterial growth and is commonly used as a standard inoculum concentration to be followed by bacterial inactivation [34–36]. Petri dishes with bovine agar were prepared for sampling by applying a 10-fold serial dilution with sample volumes of 50 µL each for the concentrate and a total sample volume of 500 µL for the permeate. Samples of the membrane surface were taken with a swab before the experiment and after 90 min and applied on the agar for cultivation. Further samples were taken from the reactor (concentrate) at 0, 30, 60 and 90 min, and afterwards from the peristaltic pump (permeate). Permeate volumes were measured separately every 30 min, showing a constant flow. The Petri dishes with the samples were stored in an incubator at 36 °C for 48 h.

3. Results and Discussion

3.1. Fouling and Self-Cleaning Properties

Several batches of UWWTP effluents were filtered through the TiO_2-ZrO_2 UF membrane. The turbidity varied from 8.7 to 21.3 NTU. During filtration to a concentration factor (CF) of 2, the pH of the concentrate slightly increased. The resulting permeate turbidity range, measured periodically from the start of the experiment to CF = 2, was 0.4 to 0.6 NTU. The TSS values of the different permeate volumes varied from 0.6 to 1.3 mg/L.

The membrane's self-cleaning capabilities were determined by continuously filtering the UWWTP effluents for 6 h (Figure 3a). The severely fouled membrane was then placed in a beaker under simulated sunlight with demineralized water and stirred lightly. The beaker was placed in the center of the solar simulator at the above irradiation settings

for 1 h to remove the fouling (Figure 3b). Irradiation continued for 2 h (Figure 3c) and 3 h (Figure 3d), showing continuous cleaning of the membrane, although not reaching its original condition, as shown in Figure 3e.

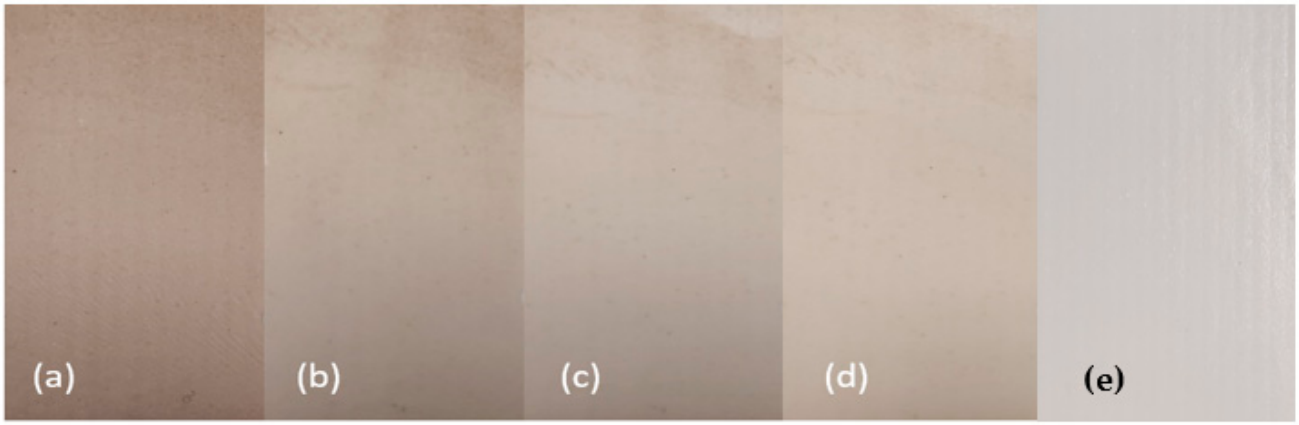

Figure 3. Membrane surface cleaning in demineralized water in the solar simulator. Pictures taken by conventional photography of the surface: (**a**) fouling color after 6 h of UWWTP effluent filtration, (**b**) after 1 h, (**c**) 2 h and (**d**) 3 h of irradiation, and (**e**) fresh membrane surface.

A clear difference from the originally severely fouled state can be observed after three 1 h irradiation periods. As a control test, another fouled membrane sample was first rinsed and placed in demineralized water but without illumination, then lightly stirred for three hours. Even after manual cleaning, membrane fouling could not be removed, demonstrating the self-cleaning effects of the photocatalytic membrane surface under irradiation. Both the original state of the fouled membrane (Figure 4a) and the membrane after 3 h of self-cleaning under simulated solar irradiation were further assessed by SEM (Figure 4b). Figure 4a is dark gray due to the presence of organic material and fouling. The presence of organic material was confirmed by EDX as having an atomic percentage of carbon of over 90%. Figure 4b shows the membrane surface with a dark spot of residual fouling in the middle. The surrounding area is the TiO_2 layer. The light-white area in the upper left corner is a minor defect of the TiO_2 layer due to previous manual cleaning.

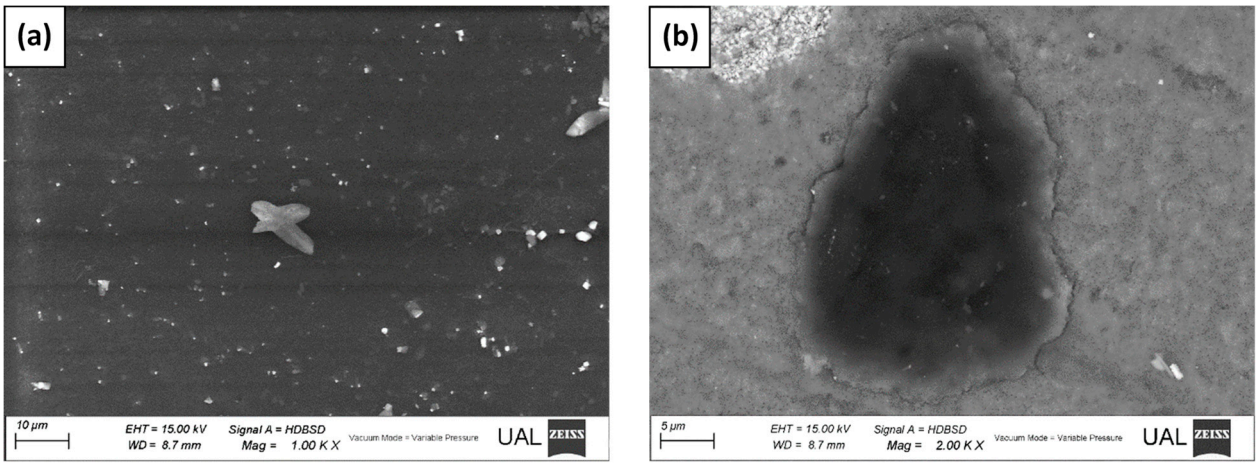

Figure 4. SEM images of the membrane after 6 h of filtration (**a**) and after cleaning for 3 h under simulated solar irradiation (**b**).

After observing a clear visual difference in the state of fouling, its physical removal—that is, recovery of most of the membrane porosity and not just a change in color—was confirmed in filtration experiments. Here, 250 mL filtered samples were taken, and the

time necessary to obtain this amount was recorded to determine whether the time needed to filter a certain volume could be affected by cleaning and whether the original filtration capability could be reached (see Figure 5). The normalized flow is shown in Figure 5 to the demonstrate change in flow rate based on the original flow and how it slows down for the reasons stated below. In both cases, a clear difference in flow rate can be seen between the membrane kept in the dark and under light during filtration. This again demonstrates the self-cleaning capabilities of the photocatalytic membrane when filtering UWWTP effluents.

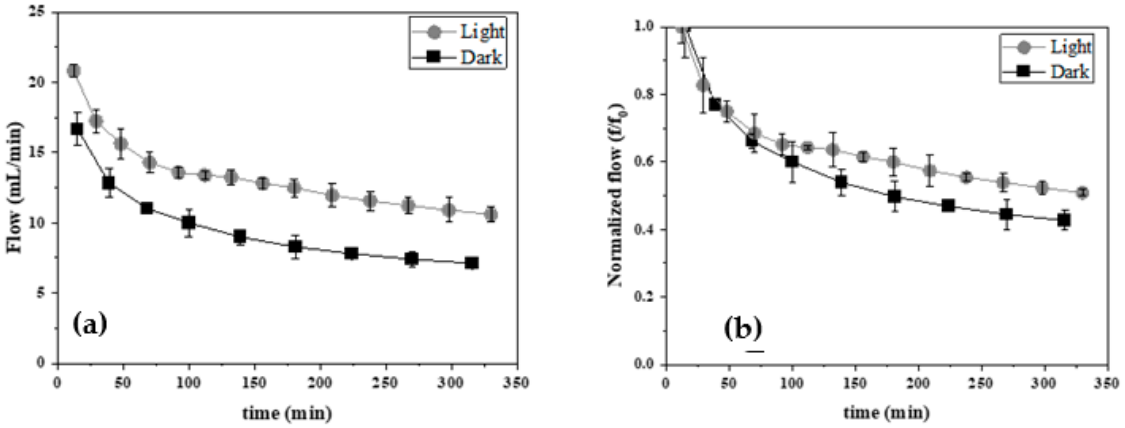

Figure 5. Filtration experiments with UWWTP effluent: (**a**) flow rates (mL/min) in the dark and in the light; (**b**) normalized flow rates (f/f_0) in the dark and in the light.

The original flow rate of 21 mL/min through the membrane in the light can be observed to be higher than the 17 mL/min rate in the dark. This can be attributed to irradiation of the membrane inhibiting attachment of suspended matter in the UWWTP effluent on the photocatalytic membrane surface. Another phenomenon is photo-induced super-hydrophilicity (PSH) of TiO_2, resulting in higher flow rates and less fouling, as also previously observed [28] and reported elsewhere [37,38]. Strong decreases in flow rate can be observed up to around 60 min, both in the light and in the dark, as fouling builds up inside the membrane pores where irradiated light cannot reach. From 60 to 120 min, a clear difference can be observed in the curve of the normalized flow rate in the light (Figure 5b), strongly suggesting that there is no photodegradation of fouling on the outer membrane surface in the dark experiment. After 120 min, the curve of filtration under radiation follows the same trend as the curve of filtration in the dark, suggesting that both membranes follow a similar trend in internal fouling, while the outer surface of the illuminated membrane is kept clean. Here, 1 L of permeate is generated in 120 min of operation in the dark.

The next step involved the observation of the effects of self-cleaning on the fouled membrane after 60 of minutes irradiation, which is considered the necessary filtration time, because this is when the curve of the normalized flow in the light deviates from the normalized flow in the dark. Furthermore, over this time, the UWWTP effluent was also spiked with 100 µg/L of each of the target MCs, namely CAF, IMI, THI, CBZ and DCF.

Figure 6 shows the flow rate during the first filtration of 1 L of UWWTP effluent in the dark. Then, the membrane was cleaned for 60 min without filtration under illumination. The second period began after this, with further filtration of 2 L of UWWTP effluent in the dark, followed by cleaning again using the same procedure followed by a third filtration. It was demonstrated that filtration of a certain volume of UWWTP effluent in the dark is possible only up to a certain amount of fouling, although the original conditions can then be recovered after illumination. However, after filtering a larger volume of UWWTP effluent, fouling could become irreversible, emphasizing the need for the definition and optimization of operating variables when using photocatalytic membranes to maintain their self-cleaning capability. There was no retention of MCs due to the high porosity of

the photocatalytic membrane, and there was no difference in the operation of membranes with UWWTP effluent, with or without MCs, as most of the fouling was eliminated by self-cleaning.

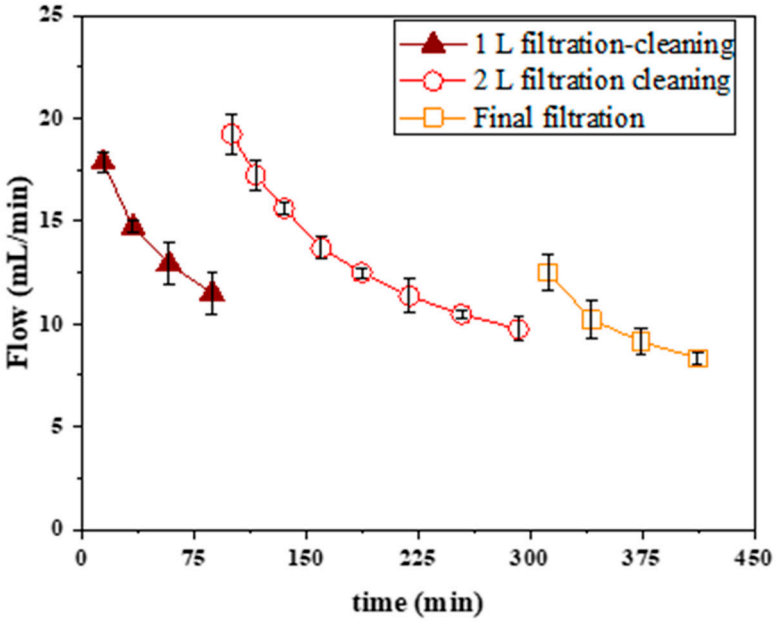

Figure 6. Filtration in the dark with self-cleaning under illumination series of UWWTP effluent spiked with 100 g/L of each MC. Note: ▲, filtration of 1 L, followed by cleaning (60 min); ○, after cleaning, filtration of 2 L, followed by cleaning (60 min); '□' after cleaning, filtration again.

The self-cleaning mechanisms of the TiO_2-ZrO_2 UF membrane are not only based on the previously mentioned super-hydrophilicity. Other mechanisms that prevent fouling of different compounds on the membrane surface can be assigned to the formation of different radical species ($^{\bullet}OH$ and other) when the photocatalytic surface material is irradiated with a photon energy equal or higher than the band gap energy of the semiconductor. The produced radical species react with organics and eliminate biofouling [39]. The specific band gaps of the UF membrane lie at 2.5 and 3.1 eV, due to the mixture of TiO_2-ZrO_2, as described in previous work [28].

3.2. Solar Photo-Fenton Treatment of Membrane Streams

The effect of UWWTP effluent filtration with the photocatalytic membrane was also evaluated in later photo-Fenton treatment of both the concentrate and permeate volumes, which still contained the initial concentration of MCs, as they were not retained by the membrane. The advantage of the photocatalytic membrane lies in pretreatment of UWWTP effluents because it significantly lowers the turbidity and particle concentration, thereby improving the availability of photons for the solar photo-Fenton process. Experiments were carried out using 0.1 mM Fe:EDDS 1:1 and 1.5 mM H_2O_2 as the oxidizing agents (Figure 7). These had been found to be the optimal settings for solar photo-Fenton testing in a previous study [40].

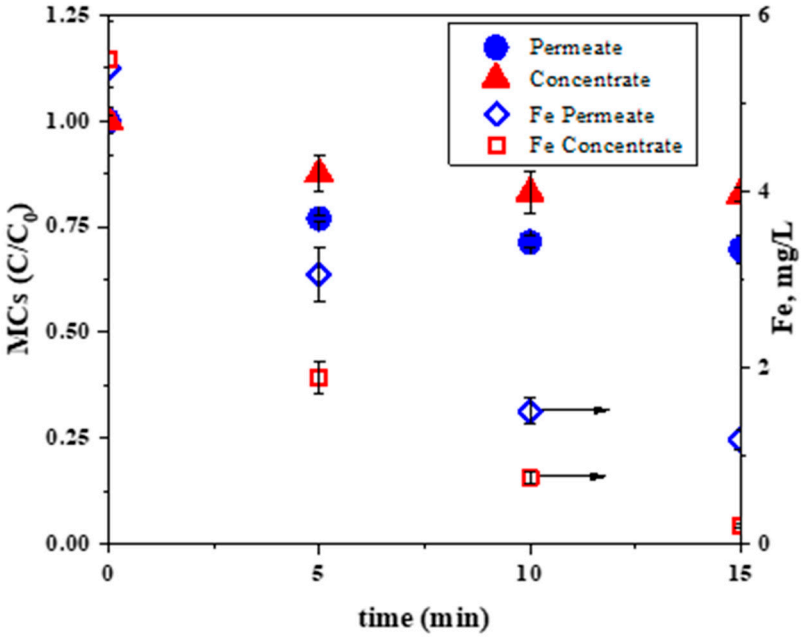

Figure 7. MC concentration (●: permeate; ▲: concentrate) in the UWWTP effluent during solar photo-Fenton treatment and the evolution of dissolved iron (◊: permeate; □: concentrate) in the solar simulator, with 0.1 mM Fe:EDDS 1:1 and 1.5 mM H_2O_2.

When the solar photo-Fenton treatment was applied to the concentrate at its natural bicarbonate concentration (720 mg/L), 16% CAF, 12% IMI, 9% THI and 27% CBZ were eliminated. DCF was already degraded by photolysis during the filtration step, or at least to below the detection limit. A total MC elimination rate of 17% was recorded, along with an H_2O_2 consumption rate of 12.5 mg/L. All dissolved iron had precipitated within 15 min, as it is well-known that the Fe-EDDS complex degrades more rapidly in the presence of particulate organic matter. The same process applied to the permeate-volume-produced MC elimination of 32% CAF, 22% IMI, 19% THI, 42% CBZ and 81% DCF, resulting in a total MC elimination rate of 32%. In this case, H_2O_2 consumption equaled 18 mg/L at the end of the experiment. The dissolved iron concentration at 15 min was higher during treatment of the permeate volume, with 22% remaining, as the Fe-EDDS complex was degraded less rapidly due to the presence of less particulate organic matter, which was removed by the self-cleaning membrane. This demonstrated that lowering the turbidity and particle concentration during filtration using self-cleaning membranes had a beneficial effect on the following photo-oxidation treatment. However, the elimination of MCs was low in both cases.

As bicarbonates are well known radical scavengers, the solar photo-Fenton process was prevented from attaining its full potential when they were present at high concentrations in the concentrate and permeate volumes, explaining the low MC elimination rates observed. This has also been observed in other studies in the literature [41,42]. Therefore, experiments were performed on the same concentrate and permeate volumes as in Figure 7, but this time after removing bicarbonates (see Figure 8). The concentrate and permeate volumes were air-stripped using H_2SO_4 to lower their initial bicarbonate concentration of 720 mg/L to 75 mg/L. During this process, the pH dropped from pH 8 to circumneutral.

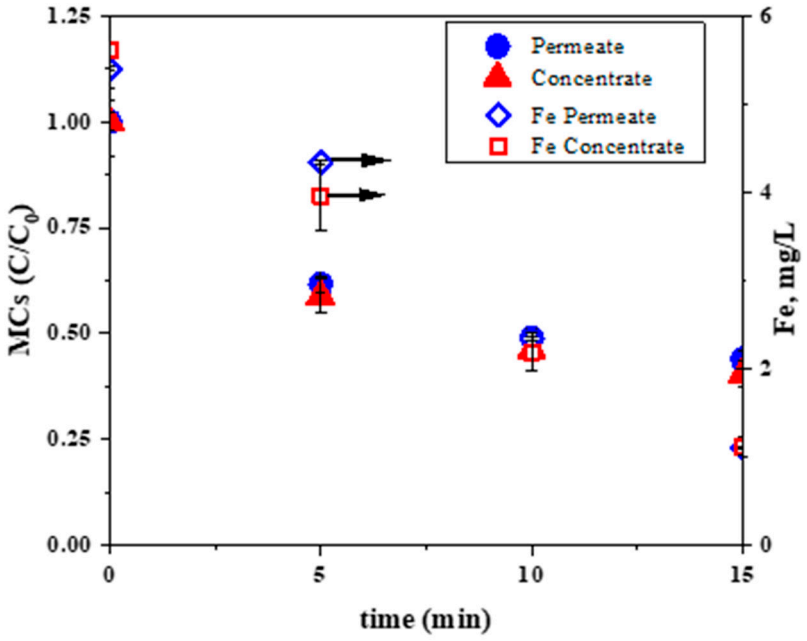

Figure 8. Evolution of MC concentration (•: permeate; ▲: concentrate) and dissolved iron (◊: permeate; □: concentrate) rates during solar photo-Fenton treatment in the solar simulator, with UWWTP effluents containing a low concentration of bicarbonates (75 mg/L) with 0.1 mM Fe:EDDS 1:1 and 1.5 mM H_2O_2.

This time the concentrate degradation efficiency was much higher, showing MC degradation of 66% CAF, 52% IMI, 45% THI and 83% CBZ. Meanwhile, DCF, as previously, was degraded by photolysis during the filtration step, or at least to below the detection limit. The total MC elimination rate was 64%, more than three times higher than with the natural concentration of bicarbonates. In addition, the H_2O_2 consumption was higher (30 mg/L), showing that dissolved iron disappeared more slowly (better stability of the Fe-EDDS complex), with 80% of iron consumed after 15 min, which was similar to the permeate volume treatment, containing its natural concentration of bicarbonates. Lower bicarbonate concentrations trigger fewer $^{\bullet}OH$ radical scavenging effects as part of the solar photo-Fenton cycle at circumneutral pH (Equations (1)–(3)) [43]. This interrupts these cycles less and regenerates the Fe(III)-EDDS complex from Fe(II)-EDDS, which is formed after quick photo degradation of the Fe(III)-EDDS complex in the first few minutes of the experiment after reacting with H_2O_2, whereas the Fe(II) also reacts with H_2O_2 to form Fe(III) and $^{\bullet}OH$ (Equation (4)) [44], explaining the higher H_2O_2 consumption rates.

$$\text{Fe(III)-EDDS} + h\nu \rightarrow \text{Fe(II)-EDDS} + H^+ \quad (1)$$

$$\text{Fe(II)-EDDS} + H_2O_2 \rightarrow \text{Fe (III)-EDDS} + {}^{\bullet}OH + HO^- \quad (2)$$

$$\text{Fe(II)-EDDS} \rightarrow \text{Fe(II)} + \text{EDDS}^{\bullet} \quad (3)$$

$$\text{Fe(II)} + H_2O_2 \rightarrow \text{Fe(III)} + {}^{\bullet}OH + HO^- \quad (4)$$

The degradation efficiency was also higher in the permeate volume, eliminating 60% CAF, 46% IMI, 39% THI, 78% CBZ and 78% DCF in 15 min. Total elimination was 59%, double that in the treatment with the natural bicarbonate concentration. This time the H_2O_2 consumption was almost three times lower, at 12.7 mg/L, attaining an iron concentration similar to the concentrate volume in 15 min, with 20% left. The lower H_2O_2 consumption can be attributed to the lower concentration of (natural) organic matter present, mainly due the lower turbidity (Section 3.1) and MC concentration profiles. Although both concentrate and permeate volumes had similar total concentrations of MCs (450 mg/L), their relative concentrations were very different, e.g., the presence and absence of DCF. Along with

differences in the type, size and morphology of the organic matter, less H_2O_2 reacted with this particulate matter, instead of being mainly consumed by the solar photo-Fenton reaction, producing $^{\bullet}OH$ without the interference of the effects of radical scavenging by bicarbonates, as the concentration was equal in both concentrate and permeate volumes. The significantly lower H_2O_2 consumption at a similar MC degradation rate shows the economic advantages of a pretreatment with the photocatalytic UF membrane. An attempt was also made to use persulfate [45] as an oxidizing agent instead of H_2O_2, at the same molar concentration, although it was found to be ineffective for the degradation of the selected MCs in the UWWTP effluent. Only 19.6% of the MCs were degraded (results not shown) compared to 64% under conventional solar photo-Fenton treatment.

3.3. Retention of P. Aeruginosa

The retention of *P. Aeruginosa* was also tested to assess future applications of the TiO_2-ZrO_2 UF membrane. Figure 9 shows the results of filtering natural water (from Tabernas, Spain; see Table S5 for physicochemical characterization) with a starting concentration of 1×10^6 CFU/mL. The membrane showed a stable flow rate of 31 mL/min over a 150 cm^2 surface. Samples were taken and prepared, as described in Section 2.3.2, and *P. Aeruginosa* CFU values were counted and calculated after 48 h of cultivation at 36 °C. Samples of the permeate volume at t = 0 min contained no *P. Aeruginosa*, or at least it was under the detection limit. Two replicates, Rep1 and Rep2, were run.

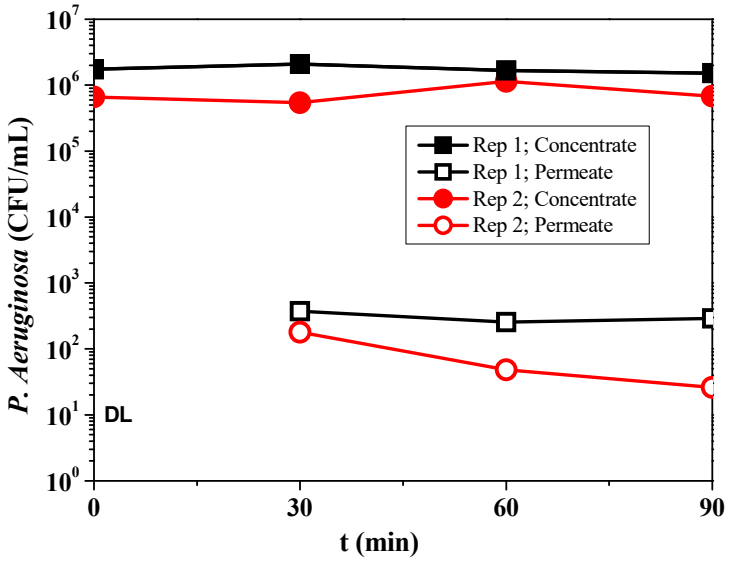

Figure 9. Retention of *P. Aeruginosa* in self-cleaning photocatalytic membranes with an initial concentration of 1×10^6 CFU/mL in natural water (Tabernas, Spain). Detection limit (DL) = 10^1.

The results in Figure 9 show that the membrane allowed the consistent retention of *P. Aeruginosa* of an order of magnitude of 1×10^3–1×10^4 CFU/mL within 90 min of filtration during Rep1 (permeate). Although the concentration of *P. Aeruginosa* in the permeate volume significantly decreased compared to the concentrate volume, lower values were expected as a function of the photocatalytic UF membrane pore size, the zirconia intermediate layer (60 nm) and the size of the rod-like *P. Aeruginosa*, which has nominal size range of 500–800 nm by 1500–3000 nm [28,46,47]. The lower-than-expected retention rate of *P. Aeruginosa* may have been due to minor damages in the photocatalytic TiO_2 membrane surface due to previous manual cleaning, as can also be observed in Figure 4b, and minor defects in the intermediate zirconia layer, making it possible for *P. Aeruginosa* to permeate the intermediate zirconia layer. However, the decreasing trend in Rep2 (permeate) in Figure 9 shows the effects (irreversible) of fouling at these sites with minor damage. A continuous fouling mechanism that can also be seen in Figure 6 resulted in a satisfactory *P. Aeruginosa* concentration in the permeate volume when operating for

more than 180 min. Certain controlled fouling mechanisms are commonly applied in ceramic membrane production and industry as a pretreatment for similar reasons.

An irradiated membrane surface would prevent the adhesion of bacteria through the abovementioned hydrophilicity, as well as degradation of any preliminary extracellular polymeric substances (EPS) produced by the bacteria to bind themselves to surfaces and for cohesion promoting protection from unfavorable conditions. Thus, the membrane would show less fouling and longer operating times. These substances can normally be observed as a slime-like biofilm layer [48].

4. Conclusions

The TiO_2-ZrO_2 ultrafiltration membrane proved to have self-cleaning capabilities when irradiated by simulated solar light after UWWTP effluents were filtered. This reduced the turbidity in the permeate by a factor of 20–50 NTU. It has been demonstrated that filtration of a certain volume of effluent in the dark is possible only up to a certain amount of fouling, then the original conditions can be recovered after illumination. However, after filtering a larger volume of effluent, fouling could become irreversible. Furthermore, the irradiated membrane showed lower fouling rates during the filtration of UWWTP effluents when irradiated. This was mainly attributed to the properties of irradiated TiO_2, including the formation of $^{\bullet}OH$, which is able to degrade microorganisms as well as microcontaminants. The TiO_2-ZrO_2 membrane significantly reduces the turbidity of the UWWTP effluent, which in turn significantly increases the degradation efficiency of the subsequent solar photo-Fenton treatment. Lowering the bicarbonate concentrations in both the concentrate and permeate resulted in higher efficiency of the solar photo-Fenton process.

The membrane shows retention of *P. Aeruginosa* to an order of magnitude of 1×10^3–1×10^4 CFU/mL. The positive effects on retention of fouling of the larger pores and minor defects can be seen when repeating short term filtration experiments. Longer filtration with the TiO_2-Zirconia ultrafiltration membrane could have positive effects on the retention of microorganisms, which would then be reversible after illumination.

Supplementary Materials: The following supporting information can be downloaded at: https://www.mdpi.com/article/10.3390/catal12050552/s1, Table S1: Composition of Urban Wastewater Treatment Plant Effluent; Table S2: Schematic overview of molecular structures of selected MCs; Table S3: Molecular weight, UPLC column retention time, LOQ and maximum contaminant absorption; Table S4: Overview of oxidation treatments and their parameters; Table S5: Composition of natural water (Tabernas, Spain).

Author Contributions: Conceptualization, D.D., I.O. and S.M.; methodology, D.D.; investigation, D.D. and F.E.B.C.; data curation, D.D. and F.E.B.C.; writing—original draft preparation, D.D. and F.E.B.C.; writing—review and editing, D.D., I.O., S.M. and A.M.A.; supervision, S.M. and A.M.A.; project administration, I.O.; funding acquisition, I.O., S.M. and A.M.A. All authors have read and agreed to the published version of the manuscript.

Funding: This paper is part of a project funded by the European Union's Horizon 2020 Research and Innovation Programme under Marie Skłodowska-Curie Grant Agreement No. 765860. The authors wish to thank the Spanish Ministry of Science, Innovation and Universities (MCIU), AEI and FEDER for funding under the CalypSol Project (Ref: RTI2018-097997-B-C32 and RTI2018-097997-B-C31).

Data Availability Statement: Not Applicable.

Acknowledgments: Dennis Deemter would like to thank the staff at the Plataforma Solar de Almería.

Conflicts of Interest: The authors declare no conflict of interest.

Abbreviations

AMR	Antimicrobial resistance
AOPs	Advanced oxidation processes
CAF	Caffeine
CBZ	Carbamazepine
CF	Concentration factor
CPC	Compound parabolic collector
DCF	Diclofenac
EDDS	Ethylenediamine-*N*: *N*′-disuccinic acid
EDX	Energy-dispersive X-ray spectroscopy
EPS	Extracellular polymeric substances
IC	Inorganic carbon
IMI	Imidacloprid
LOQ	Limit of quantification
MCs	micro contaminants
NF	Nanofiltration
PSH	Photo-induced super-hydrophilicity
RO	Reverse osmosis
SEM	Scanning electron microscopy
THI	hiacloprid
TOC	Total organic carbon
TSS	Total suspended solids
UF	Ultrafiltration
UWW	Urban wastewater
UWWTP	Urban wastewater treatment plant

References

1. Messaoudi, M.; Douma, M.; Tijani, N.; Messaoudi, L. Study of the permeability of tubular mineral membranes: Application to wastewater treatment. *Heliyon* **2021**, *7*, e06837. [CrossRef] [PubMed]
2. Gao, Y.; Zhang, Y.; Dudek, M.; Qin, J.; Gisle, Ø.; Stein, W.Ø. A multivariate study of backpulsing for membrane fouling mitigation in produced water treatment. *J. Environ. Chem. Eng.* **2021**, *9*, 104839. [CrossRef]
3. Alawad, S.M.; Khalifa, A.E. Case Studies in Thermal Engineering Development of an efficient compact multistage membrane distillation module for water desalination. *Case Stud. Therm. Eng.* **2021**, *25*, 100979. [CrossRef]
4. Comas, J.; Corominas, L. Balancing environmental quality standards and infrastructure upgrade costs for the reduction of microcontaminant loads in rivers. *Wat. Res.* **2018**, *143*, 632–641. [CrossRef]
5. de Santiago-martín, A.; Meffe, R.; Teijón, G.; Martínez, V.; López-heras, I.; Alonso, C.; Arenas, M.; de Bustamante, I. Pharmaceuticals and trace metals in the surface water used for crop irrigation: Risk to health or natural attenuation? *Sci. Total Environ.* **2020**, *705*, 135825. [CrossRef]
6. Asghar, A.; Lutze, H.V.; Tuerk, J.; Schmidt, T.C. Influence of water matrix on the degradation of organic micropollutants by ozone based processes: A review on oxidant scavenging mechanism. *J. Hazard. Mater.* **2022**, *429*, 128189. [CrossRef]
7. Ribeiro, J.P.; Nunes, M.I. Recent trends and developments in Fenton processes for industrial wastewater treatment—A critical review. *Environ. Res.* **2021**, *197*, 110957. [CrossRef]
8. Du, X.; Oturan, M.A.; Zhou, M.; Belkessa, N.; Su, P.; Cai, J.; Trellu, C.; Mousset, E. Nanostructured electrodes for electrocatalytic advanced oxidation processes: From materials preparation to mechanisms understanding and wastewater treatment applications. *Appl. Catal. B Environ.* **2021**, *296*, 120332. [CrossRef]
9. Rizzo, L.; Malato, S.; Antakyali, D.; Beretsou, V.G.; Đolić, M.B.; Gernjak, W.; Heath, E.; Ivancev-Tumbas, I.; Karaolia, P.; Ribeiro, A.R.L.; et al. Consolidated vs new advanced treatment methods for the removal of contaminants of emerging concern from urban wastewater. *Sci. Total Environ.* **2019**, *655*, 986–1008. [CrossRef]
10. Bouzerara, F.; Guvenc, C.M.; Demir, M.M. Fabrication and properties of novel porous ceramic membrane supports from the (Sig) diatomite and alumina mixtures. *Bol. Soc. Esp. Cerám. Vidr.* 2021; 1–10, *in press*. [CrossRef]
11. Zsirai, T.; Qiblawey, H.; Ahmed, A.; Bach, S.; Watson, S.; Judd, S. Ceramic membrane filtration of produced water: Impact of membrane module. *Sep. Purif. Technol.* **2016**, *165*, 214–221. [CrossRef]
12. da Silva Biron, D.; Dos Santos, V.; Zeni, M. *Ceramic Membranes Applied in Separation Processes*; Springer: Berlin/Heidelberg, Germany, 2017. [CrossRef]
13. Gitis, V.; Rothenberg, G. *Ceramic Membranes: Ceramic Membranes: New Opportunities and Practical Applications*; John Wiley & Sons: Hoboken, NJ, USA, 2016. [CrossRef]

14. Zhang, L.; Xu, L.; Graham, N.; Yu, W. Unraveling membrane fouling induced by chlorinated water versus surface water: Biofouling properties and microbiological investigation. *Engineering*, 2021; *in press*. [CrossRef]
15. Hoslett, J.; Maria, T.; Malamis, S.; Ahmad, D.; van den Boogaert, I.; Katsou, E.; Ahmad, B.; Ghazal, H.; Simons, S.; Wrobel, L.; et al. Science of the Total Environment Surface water fi ltration using granular media and membranes: A review. *Sci. Total Environ.* **2018**, *639*, 1268–1282. [CrossRef] [PubMed]
16. Czuba, K.; Bastrzyk, A.; Rogowska, A.; Janiak, K.; Pacyna, K.; Kossi, N.; Podstawczyk, D. Towards the circular economy—A pilot-scale membrane technology for the recovery of water and nutrients from secondary effluent. *Sci. Total Environ.* **2021**, *791*, 148266. [CrossRef] [PubMed]
17. Kolesnyk, I.; Kujawa, J.; Bubela, H.; Konovalova, V.; Burban, A. Separation and Purification Technology Photocatalytic properties of PVDF membranes modi fi ed with g-C3N4 in the process of Rhodamines decomposition. *Sep. Purif. Technol.* **2020**, *250*, 117231. [CrossRef]
18. Della-Flora, A.; Wilde, M.L.; Thue, P.S.; Lima, D.; Lima, E.C.; Sirtori, C. Combination of solar photo-Fenton and adsorption process for removal of the anticancer drug Flutamide and its transformation products from hospital wastewater. *J. Hazard. Mater.* **2020**, *396*, 122699. [CrossRef]
19. Foteinis, S.; Monteagudo, J.M.; Durán, A.; Chatzisymeon, E. Environmental sustainability of the solar photo-Fenton process for wastewater treatment and pharmaceuticals mineralization at semi-industrial scale. *Sci. Total Environ.* **2018**, *612*, 605–612. [CrossRef]
20. Li, Y.; Cheng, H. Chemical kinetic modeling of organic pollutant degradation in Fenton and solar photo-Fenton processes. *J. Taiwan Inst. Chem. Eng.* **2021**, *123*, 175–184. [CrossRef]
21. Norén, A.; Fedje, K.K.; Strömvall, A.-M.; Rauch, S.; Andersson-Sköld, Y. Low impact leaching agents as remediation media for organotin and metal contaminated sediments. *J. Environ. Manag.* **2021**, *282*, 111906. [CrossRef]
22. Vandevivere, P.C.; Saveyn, H.; Verstraete, W.; Feijtel, T.C.J.; Schowanek, D.R. Biodegradation of metal-[S,S]-EDDS complexes. *Environ. Sci. Technol.* **2001**, *35*, 1765–1770. [CrossRef]
23. Clarizia, L.; Russo, D.; di Somma, I.; Marotta, R.; Andreozzi, R. Homogeneous photo-Fenton processes at near neutral pH: A review. *Appl. Catal. B Environ.* **2017**, *209*, 358–371. [CrossRef]
24. Vineyard, D.; Hicks, A.; Karthikeyan, K.G.; Barak, P. Economic analysis of electrodialysis, denitri fi cation, and anammox for nitrogen removal in municipal wastewater treatment. *J. Clean. Prod.* **2020**, *262*, 121145. [CrossRef]
25. Igere, B.E.; Okoh, A.I.; Nwodo, U.U. Wastewater treatment plants and release: The vase of Odin for emerging bacterial contaminants, resistance and determinant of environmental wellness. *Emerg. Contam.* **2020**, *6*, 212–224. [CrossRef]
26. del Mar Cendra, M.; Torrents, E. Pseudomonas aeruginosa biofilms and their partners in crime. *Biotechnol. Adv.* **2021**, *49*, 107734. [CrossRef] [PubMed]
27. Rizzo, L.; Gernjak, W.; Krzeminski, P.; Malato, S.; McArdell, C.S.; Perez, J.A.S.; Schaar, H.; Fatta-Kassinos, D. Best available technologies and treatment trains to address current challenges in urban wastewater reuse for irrigation of crops in EU countries. *Sci. Total Environ.* **2020**, *710*, 136312. [CrossRef] [PubMed]
28. Coelho, F.E.B.; Deemter, D.; Candelario, V.M.; Boffa, V.; Malato, S.; Magnacca, G. Development of a Photocatalytic Zirconia-Titania Ultrafiltration Membrane with Anti-fouling and Self-cleaning Properties. *J. Environ. Chem. Eng.* **2021**, *9*, 106671. [CrossRef]
29. Federal Office for the Environment FOEN Water Division. *Reporting for Switzerland under the Protocol on Water and Health*. 2019. Available online: https://unece.org/DAM/env/water/Protocol_reports/reports_pdf_web/Switzerland_summary_report_en.pdf (accessed on 12 May 2022).
30. Hosseinkhan, N.; Allahverdi, A.; Abdolmaleki, F. The novel potential multidrug-resistance biomarkers for Pseudomonas aeruginosa lung infections using transcriptomics data analysis. *Informatics Med. Unlocked.* **2021**, *22*, 100509. [CrossRef]
31. Horna, G.; Ruiz, J. Type 3 secretion system of Pseudomonas aeruginosa. *Microbiol. Res.* **2021**, *246*, 126719. [CrossRef]
32. Shaker, M.M.; Al-Hadrawi, H.A.N. Measuring the effectiveness of antibiotics against Pseudomonas aeruginosa and Escherichia coli that isolated from urinary tract infection patients in Al-Najaf city in Iraq. *Mater. Today Proc. in press* **2021**, 10–13. [CrossRef]
33. Liang, C.; Huang, C.F.; Mohanty, N.; Kurakalva, R.M. A rapid spectrophotometric determination of persulfate anion in ISCO. *Chemosphere* **2008**, *73*, 1540–1543. [CrossRef]
34. Lozano, C.; López, M.; Rojo-Bezares, B.; Sáenz, Y. Antimicrobial susceptibility testing in pseudomonas aeruginosa biofilms: One step closer to a standardized method. *Antibiotics* **2020**, *9*, 880. [CrossRef]
35. Díez-Aguilar, M.; Martínez-García, L.; Cantón, R.; Morosini, M.I. Is a new standard needed for diffusion methods for in vitro susceptibility testing of fosfomycin against Pseudomonas aeruginosa? *Antimicrob. Agents Chemother.* **2016**, *60*, 1158–1161. [CrossRef]
36. Mizunaga, S.; Kamiyama, T.; Fukuda, Y.; Takahata, M.; Mitsuyama, J. Influence of inoculum size of Staphylococcus aureus and Pseudomonas aeruginosa on in vitro activities and in vivo efficacy of fluoroquinolones and carbapenems. *J. Antimicrob. Chemother.* **2005**, *56*, 91–96. [CrossRef]
37. Kim, S.M.; In, I.; Park, S.Y. Study of photo-induced hydrophilicity and self-cleaning property of glass surfaces immobilized with TiO_2 nanoparticles using catechol chemistry. *Surf. Coatings Technol.* **2016**, *294*, 75–82. [CrossRef]
38. Saini, A.; Arora, I.; Ratan, J.K. Photo-induced hydrophilicity of microsized-TiO_2 based self-cleaning cement. *Mater. Lett.* **2020**, *260*, 26888. [CrossRef]

39. Rani, C.N.; Karthikeyan, S.; Arockia, S.P. Photocatalytic ultrafiltration membrane reactors in water and wastewater treatment—A review. *Chem. Eng. Process. Process Intensif.* **2021**, *165*, 108445. [CrossRef]
40. Deemter, D.; Oller, I.; Amat, A.M.; Malato, S. Effect of salinity on preconcentration of contaminants of emerging concern by nanofiltration: Application of solar photo-Fenton as a tertiary treatment. *Sci. Total Environ.* **2020**, *756*, 143593. [CrossRef]
41. Rommozzi, E.; Giannakis, S.; Giovannetti, R.; Vione, D.; Pulgarin, C. Detrimental vs. beneficial influence of ions during solar (SODIS) and photo-Fenton disinfection of *E. coli* in water: (Bi)carbonate, chloride, nitrate and nitrite effects. *Appl. Catal. B Environ.* **2020**, *270*, 118877. [CrossRef]
42. Gonçalves, B.R.; Guimarães, R.O.; Batista, L.L.; Ueira-Vieira, C.; Starling, M.C.V.M.; Trovó, A.G. Reducing toxicity and antimicrobial activity of a pesticide mixture via photo-Fenton in different aqueous matrices using iron complexes. *Sci. Total Environ.* **2020**, *740*, 140152. [CrossRef] [PubMed]
43. Soriano-Molina, P.; Sánchez, J.L.G.; Malato, S.; Pérez-Estrada, L.A.; Pérez, J.A.S. Effect of volumetric rate of photon absorption on the kinetics of micropollutant removal by solar photo-Fenton with Fe^{3+}-EDDS at neutral pH. *Chem. Eng. J.* **2018**, *331*, 84–92. [CrossRef]
44. Li, J.; Mailhot, G.; Wu, F.; Deng, N. Journal of Photochemistry and Photobiology A: Chemistry Photochemical efficiency of Fe (III)-EDDS complex: OH radical production. *J. Photochem. Photobiol. A Chem.* **2010**, *212*, 1–7. [CrossRef]
45. Kanafin, Y.N.; Makhatova, A.; Zarikas, V.; Arkhangelsky, E.; Poulopoulos, S.G. Photo-Fenton-Like Treatment of Municipal Wastewater. *Catalysts* **2021**, *11*, 1206. [CrossRef]
46. Iglewski, B. Pseudomonas. In *Medical Microbiology*, 4th ed.; Baron, S., Ed.; The University of Texas: Galveston, TX, USA, 1996. Available online: https://www.ncbi.nlm.nih.gov/books/NBK8326/%0A (accessed on 12 May 2022).
47. Formosa, C.; Grare, M.; Duval, R.E.; Dague, E. Nanoscale effects of antibiotics on *P. aeruginosa*. *Nanomed. Nanotechnol. Biol. Med.* **2012**, *8*, 12–16. [CrossRef] [PubMed]
48. Harimawan, A.; Ting, Y. Colloids and Surfaces B: Biointerfaces Investigation of extracellular polymeric substances (EPS) properties of *P. aeruginosa* and *B. subtilis* and their role in bacterial adhesion. *Colloids Surf. B Biointerfaces* **2016**, *146*, 459–467. [CrossRef] [PubMed]